Biosensors and Bioelectronics 59 (2014) 350–357

Contents lists available at ScienceDirect

Biosensors and Bioelectronics

journal homepage: www.elsevier.com/locate/bios

Zinc oxide inverse opal electrodes modified by glucose oxidase for electrochemical and photoelectrochemical biosensor

Lei Xia, Jian Song, Ru Xu, Dali Liu *, Biao Dong, Lin Xu, Hongwei Song **

State Key Laboratory on Integrated Optoelectronics, College of Electronic Science and Engineering, Jilin University, 2699 Qianjin Street, Changchun 130012, China

ARTICLE INFO

Article history:
Received 1 March 2014
Received in revised form
18 March 2014
Accepted 19 March 2014
Available online 29 March 2014

Keywords:
ZnO inverse opal photonic crystals
ZnO IOPCs modified FTO electrode
Glucose oxidase
Electrochemical biosensor
Photoelectrochemical biosensor

ABSTRACT

The ZnO inverse opal photonic crystals (IOPCs) were synthesized by the sol–gel method using the polymethylmethacrylate (PMMA) as a template. For glucose detection, glucose oxidase (GOD) was further immobilized on the inwall and surface of the IOPCs. The biosensing properties toward glucose of the Nafion/GOD/ZnO IOPCs modified FTO electrodes were carefully studied and the results indicated that the sensitivity of ZnO IOPCs modified electrode was 18 times than reference electrode due to the large surface area and uniform porous structure of ZnO IOPCs. Moreover, photoelectrochemical detection for glucose using the electrode was realized and the sensitivity approached to 52.4 $\mu A\ mM^{-1}\ cm^{-2}$, which was about four times to electrochemical detection (14.1 $\mu A\ mM^{-1}\ cm^{-2}$). It indicated that photoelectrochemical detection can highly improve the sensor performance than conventional electrochemical method. It also exhibited an excellent anti-interference property and a good stability at the same time. This work provides a promising approach for realizing excellent photoelectrochemical biosensor of similar semiconductor photoelectric material.

1. Introduction

Glucose biosensors, one of the most commonly used biosensors, have been widely investigated and developed due to its important application in the field of clinical detection, biological analysis, environmental monitor and food industry (Asif et al., 2010; Fang et al., 2009; Rakow and Suslick, 2000). Glucose oxidase (GOD) is often used as the enzyme in glucose amperometric biosensors to catalyze the oxidation of glucose because of its high selectivity, fast response, and low cost (Lee et al., 2005; Wang and Joseph, 2008). However, the GOD modified bare electrodes are hard to achieve its activity and stability (Mu et al., 2007; Riklin et al., 1995). Therefore, synthesizing and immobilizing functional materials on an electrode surface is necessary in novel biosensor design. Among conventional materials, the inorganic materials with nanostructure could provide large surface to volume ratio and remain activity of biomolecules, which is important for enzymatic immobilization and electron transmissions (Zhang et al., 2004). In recent years, although many different inorganic nanomaterials, such as gold nanoparticles and nanoclusters (Zhang et al., 2005; Zhao et al., 2006), carbon nanotube (Liu et al., 2005), Ag dendritic nanostructures (Wen et al., 2006), Au/polyaniline nanocomposite (Xian et al., 2006), calcium carbonate nanoparticles (Shan et al., 2007), have been studied as platforms for immobilizing biomolecules and transferring electrons, there is still a great challenge to develop new structural materials for better activity, specificity, and stability for super bioelectrocatalysis.

ZnO nanomaterials, a classic and widely used wide-and-gap semiconductor, possess several unique advantages for biosensor application, such as high specific surface area, nontoxicity, good biocompatibility, chemical stability, and high electron communication features (Zhang et al., 2004; Zhu et al., 2007; Hu et al., 2010; Wang et al., 2006; Umar et al., 2008; Wei et al., 2006). Moreover, ZnO has a high isoelectric point (IEP) of about 9.5, which can play as a positively charged substrate for immobilization of low IEP proteins or enzyme such as GOD (IEP ≈ 4.2) at the physiological pH of 7.4 by electrostatic interactions (Arpin et al., 2010).

Many varieties of ZnO nanostructures, including nanorods (Hu et al., 2010), nanocombs (Wang et al., 2006), nanotubes (Dai et al., 2009), nanoclusters (Zhao et al., 2007), hollow nanospheres (Fang et al., 2011), nanonails (Umar et al., 2008) and nanowires (Zang et al., 2007), have been reported to immobilize GOD for electrochemical determination of glucose.

Here, ZnO IOPCs were synthesized for an electrochemical and photoelectrochemical biosensor. The structure of IOPCs, which has a large surface area and a uniform porous distribution, is conducive to the electronic transmission and the enzyme adsorption. The porous structure may shorten the electronic diffuse distance

* Corresponding author. Fax: +86 431 8516 8270.
** Corresponding author. Fax: +86 431 8515 5129.
E-mail addresses: ldl@jlu.edu.cn (D. Liu), songhw@jlu.edu.cn (H. Song).

http://dx.doi.org/10.1016/j.bios.2014.03.038
0956-5663/

between the FTO substrate and the redox centers of the immobilized proteins, thus promoting the electron transfer ability from the redox protein to the electrode surface (Zhu et al., 2005; Yang et al., 1998). Moreover, the structure of IOPCs can increase the light absorption of certain wavelength, which may enhance the sensitivity in photoelectrochemical detection.

Photonic crystal is a periodic dielectric structure that can forbid the propagation of light in a certain crystal direction within a certain spectrum regime, called a photonic stop band (PSB) (Joannopoulos et al., 2008). The light in a PC undergoes strong coherent multiple scattering and travels with very low group velocity near the PSB edges, referred to as slow light (Sakoda, 1999). The slow light effect can considerably increase the effective optical path length, therefore leading to a delay and storage of light in photonic materials (Baba, 2008). The slow light effect on photovoltaic cells and the photochemical process was investigated by Nishimura (Nishimura et al., 2003) and Chen (Chen et al., 2006, 2007, 2008) as a means of promoting the optical absorbance of the TiO_2-based composite system. Since then, the effect has been utilized for the enhancement in efficiencies of dye-sensitized TiO_2 solar cells and photocatalytic reaction (Lee et al., 2008; Liao et al., 2010; Chen et al., 2010a,b). Considering the superiorities of ZnO nanometerials as a photoanode material, if slow light propagating in the ZnO IOPCs structure is designed to be resonant with a specific light frequency around its electronic absorption edge, the interaction with ZnO and light should be greatly increased. To our knowledge, there is yet no study available on improving the sensitivity of glucose detection by a photoelectrochemical sensor using ZnO IOPCs electrodes.

In this work, we prepared ZnO IOPCs by a facile template method, and then fabricated the Nafion/GOD/ZnO IOPCs modified FTO electrodes by modifying GOD and Nafion successively. In addition, we realized photoelectrochemical detection for glucose and observed highly improved sensing properties.

2. Results and discussion

2.1. Material characterization

Scheme 1a illustrates the fabricated process of a Nafion/GOD/ZnO IOPCs modified FTO electrode. The surface morphology and microstructure of the synthesized ZnO IOPCs were characterized by field emission scanning electron microscope (SEM) and

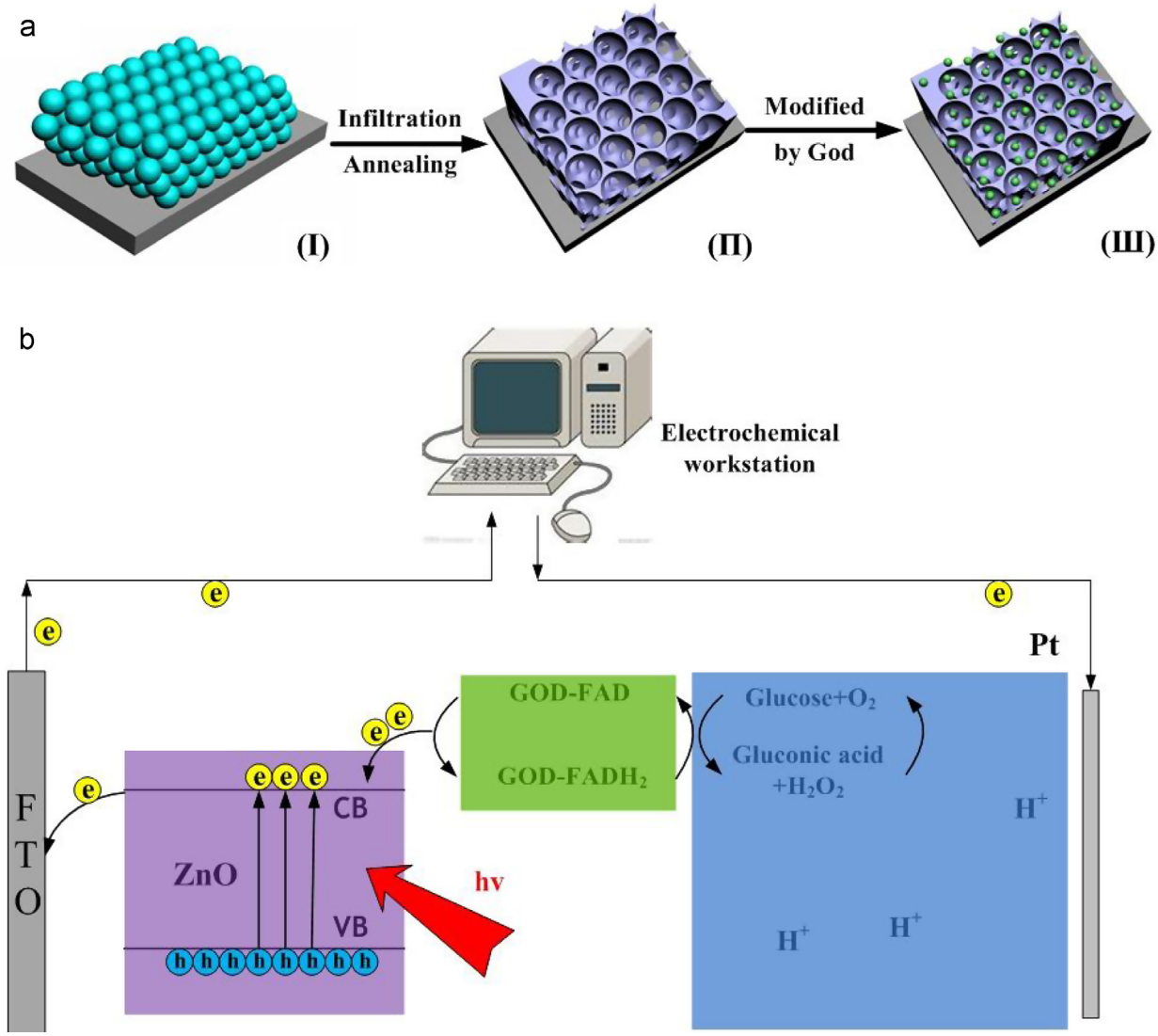

Scheme 1. (a) Schematic illustration for the synthesis of the Nafion/GOD/ZnO IOPCs modified FTO electrode. (b) Schematic illustration for the reaction process of the Nafion/GOD/ZnO IOPCs modified FTO electrode to glucose .

transmission electron microscopy (TEM). The SEM image of the as-prepared ZnO IOPCs (Fig. 1a) showed a long-range ordered hexagonal close-packed arrangement of inverse opal structure in a three-dimensional space. To further investigate more detailed structure and morphology of ZnO IOPCs, a high-magnification TEM image was needed. Fig. 1b illustrates that the wall thickness of the ZnO IOPCs is about 20 nm, consisted of a large amount of small nanoparticles (NPs), and the neighboring pores connected each other by the ZnO thin wall, which is conductive to electrons unidirectional transmission. The large porous structure of ZnO IOPCs facilitated the entrance and adsorption of the GOD molecules (7.0 nm × 5.5 nm × 8.0 nm) (Wu et al., 2007). The large surface area of ZnO IOPCs also gave more chance for the GOD to link on its surface. As shown in Fig. 1c, the cross-section SEM images of ZnO IOPCs also exhibited vertical ordering. The thickness of the as-prepared ZnO IOPCs with face-centered-cubic (fcc) packing structure was measured as around 2.6 μm, indicating that it is a multilayer structure with more than 30 layers. The phase features of the synthesized ZnO IOPCs were investigated by X-ray powder diffraction (XRD). As shown in Fig. 1d, the XRD patterns of the ZnO IOPCs powder matched well to the hexagonal ZnO phase (JCPDS, card no. 36-1451), which suggested that the hexagonal ZnO formed during the process of annealing heat treatment. No characteristic peaks of impurities were observed, implying that the samples were ZnO in a pure hexagonal phase. When the sample was grown on the FTO substrate, only two very weak peaks of ZnO were observed, and the other main peaks could be indexed to the SnO (JCPDS, card no. 46-1088), which was the major doped components of the FTO substrate.

2.2. Enzyme immobilization on the ZnO IOPCs

The effectiveness of GOD immobilization on ZnO IOPCs was investigated by FTIR spectroscopy (Fig. 2a). The pure ZnO exhibited a intrinsic absorption band at 478 cm^{-1}, and the bands at 1640 cm^{-1} and 1045 cm^{-1} corresponded to the deformation vibration of H–O–H bonds from the adsorbed water to the stretching vibration of the Zn–O–C bond from the synthesizing process of ZnO IOPCs, respectively. For GOD, two infrared peaks with the center position at 1650 cm^{-1} and 1542 cm^{-1} could be observed, which were generally used as an indication of protein denaturation and conformational change upon immobilization (Vinu et al., 2005). The typical amide I and amide II adsorption peaks could also be observed in the GOD/ZnO sample, which suggested that the GOD retained the essential features after being adsorbed on the surface of ZnO IOPCs and revealed the good biocompatibility of ZnO. The amide adsorption peaks had a red shift to 1662 cm^{-1} and 1554 cm^{-1}, which might be due to the strong electrostatic interaction between the anchored GOD and ZnO IOPCs.

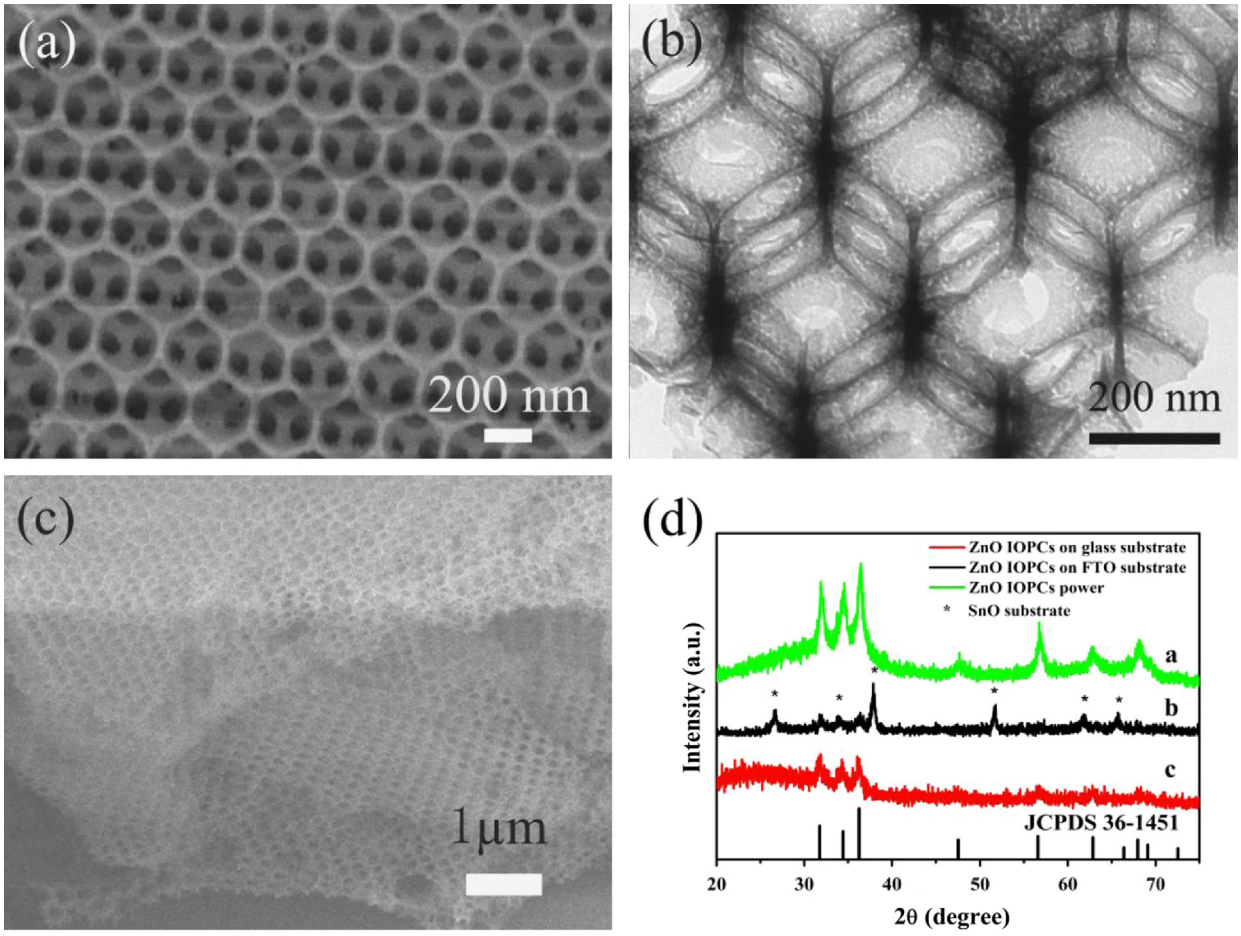

Fig. 1. (a) SEM image of ZnO IOPCs. (b) TEM image of ZnO IOPCs. (c) SEM images of cross-section view of ZnO IOPCs. (d) XRD patterns of different ZnO IOPCs samples: (a) ZnO IOPCs power (green line), (b) ZnO IOPCs on FTO substrate (black line), and (c) ZnO IOPCs on glass slide (red line). (For interpretation of the references to color in this figure caption, the reader is referred to the web version of this paper.)

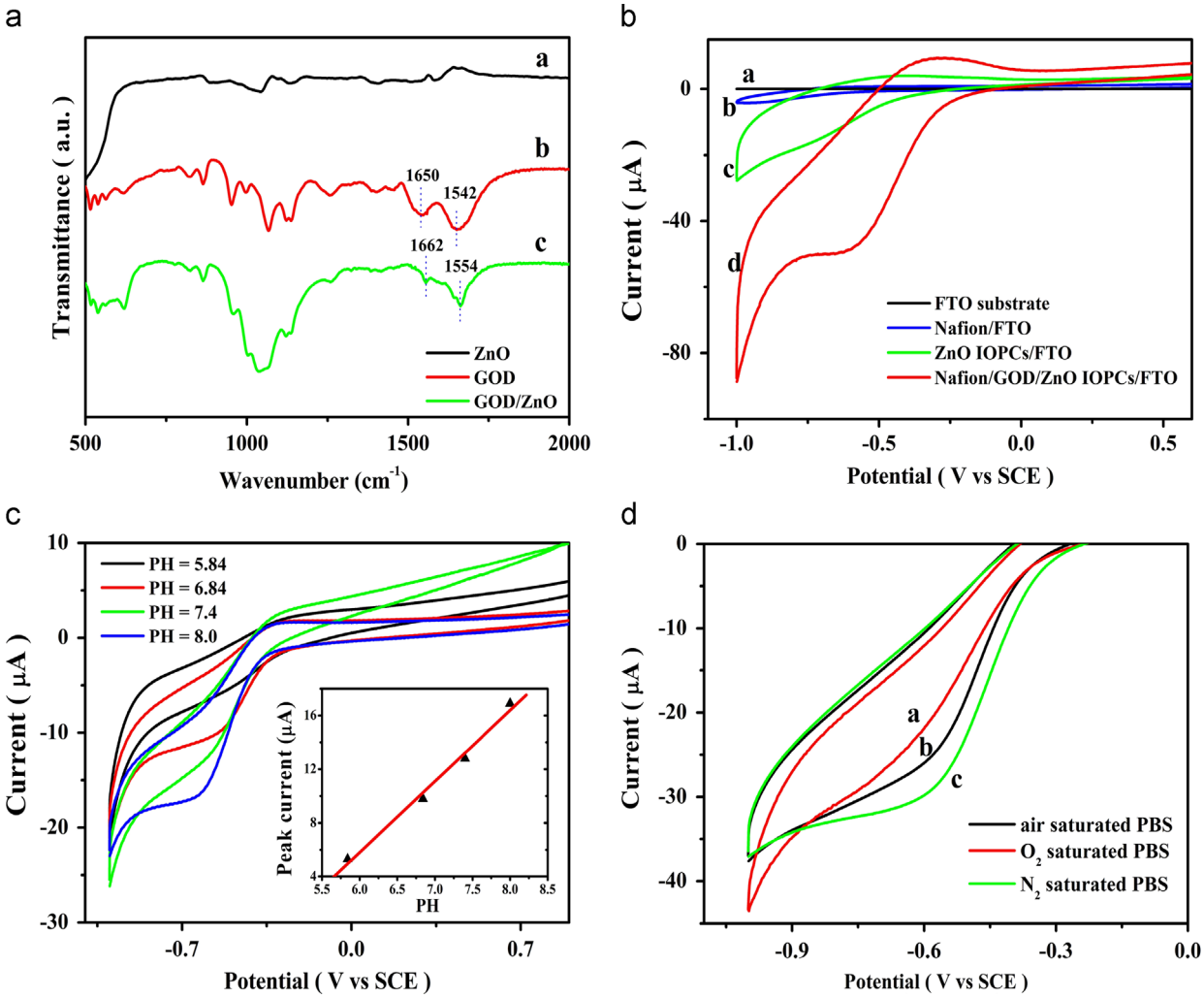

Fig. 2. (a) IR spectra of (a) ZnO IOPCs (black), (b) pure GOD (red), and (c) GOD-modified ZnO IOPCs (green). (b) CV curves of the FTO substrate, Nafion/FTO, ZnO IOPCs/FTO, and Nafion/GOD/ZnO IOPCs modified FTO electrodes in 0.1 M PBS at 50 mV s^{-1}. (c) Cyclic voltammograms of the Nafion/GOD/ZnO IOPCs modified FTO electrode with different pH value. (Inset) Plots of peak currents versus pH value. (d) Cyclic voltammograms of the Nafion/GOD/ZnO IOPCs modified FTO electrode with different conditions. (For interpretation of the references to color in this figure caption, the reader is referred to the web version of this paper.)

2.3. Electrochemistry property of Nafion/GOD/ZnO IOPCs modified FTO electrode

Scheme 1b illustrates the reaction process of the Nafion/GOD/ZnO IOPCs modified FTO electrode to glucose. To study the direct electron transfer of GOD immobilized ZnO IOPCs, cyclic voltammetry (CV) measurements were performed using FTO, Nafion/FTO, ZnO IOPCs/FTO, and Nafion/GOD/ZnO IOPCs modified FTO electrodes in 0.1 M PBS at a scan rate of 50 mV s^{-1}. As shown in Fig. 2b, there was no current response when the FTO electrode was not modified. The Nafion/FTO and ZnO IOPCs/FTO electrodes exhibited only typical square-shaped CV curves as a result of double-layer capacitance in the applied potential window, indicating that both the GOD and ZnO IOPCs were electrochemically inactive over this potential range. In contrast, a pair of well-defined redox peaks were observed in the CV curves of Nafion/GOD/ZnO IOPCs modified FTO electrodes, with a cathodic reduction peak potential (E_{pc}) of −0.648 V and an anodic oxidation peak potential (E_{pa}) of −0.30 V, which demonstrated the ability of direct electron transfer of GOD between the hosted protein and the electrode.

Cyclic voltammograms of Nafion/GOD/ZnO IOPCs modified FTO electrodes showed a strong dependence on solution pH value, as shown in Fig. 2c. Stable and well-defined CV curves could be obtained in the pH range 5.84–8.0. Negative shifts in reduction peak potentials were observed with an increase in solution pH value, which indicated that the hydrogen ions took part in the electrode reaction. The slope of the peak current versus pH value was 61.3 μA pH^{-1} (inset of Fig. 2c) (R=0.9947). The result was in accordance with the previous work and could be explained well (Bao et al., 2008). The direct electrochemistry of GOD on the electrode involved a two-proton redox reaction, as follows:

$$GOD-FAD+2e^{-}+2H^{+}\leftrightarrow GOD-FADH_2. \quad (1)$$

Fig. 2d displays the cyclic voltammograms of Nafion/GOD/ZnO IOPCs modified FTO electrodes in O_2-saturated, N_2-saturated and air-saturated 0.1 M PBS. In the presence of oxygen, the reduced enzyme (GOD–$FADH_2$) in Eq. (1) can be further oxidized by dissolved oxygen very quickly at the surface of the electrode, as follows:

$$GOD-FADH_2+O_2\rightarrow GOD-FAD+H_2O_2. \quad (2)$$

The catalytic regeneration of the enzyme in its oxidized form caused the loss of reversibility and suppressed the reduction reaction on the electrode. In other words, the electrochemically formed GOD (GOD–$FADH_2$) catalyzed the reduction of dissolved oxygen. The value of cathodic reduction peaks had obvious change, while the anodic peaks demonstrated little difference in three

conditions. The cathodic reduction peak current decreased with the increase of amount of oxygen in the solution.

The effect of scan rate on the electrochemical response of the Nafion/GOD/ZnO IOPCs modified FTO electrode is displayed in Fig. S1, indicating that the electron transfer process in the GOD redox reaction was a surface-controlled mechanism.

2.4. Amperometric detection of electrochemical and photoelectrochemical biosensor

A reference Nafion/GOD/ZnO thin film modified FTO electrode was made by a spin-coating method using the same prepared precursor solution of ZnO, and then annealed and immobilized GOD on the surface under the same condition. The ZnO IOPCs and ZnO thin film grown on the FTO had the same quality. To determine electrochemical and photoelectrochemical biosensor application, all the current–time ($I-t$) curves were obtained at an applied potential of -0.6 V versus a saturated calomel electrode reference electrode in 0.1 M PBS. A negative redox potential of the direct electrochemistry on ZnO IOPCs not only demonstrated its great electrocatalytic activity, but could also reduce the interference. This was particularly important in an implantable glucose sensor (Li et al., 2007).

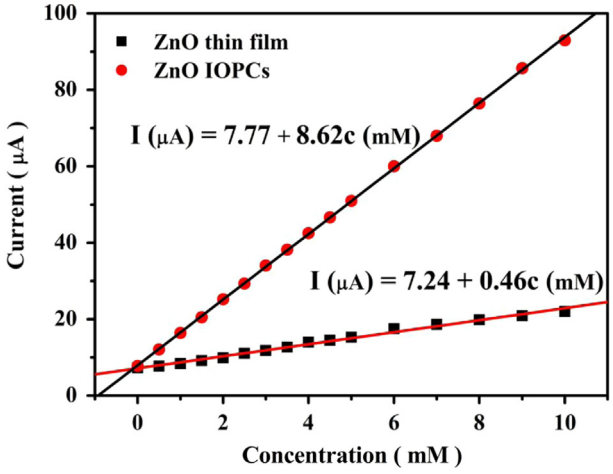

Fig. 3. Calibration curves of amperometric response of the ZnO IOPCs modified electrode and the ZnO thin film modified electrode to successive addition of glucose at an applied potential of -0.6 V.

Fig. 3 shows the electrochemical response calibration curves of the Nafion/GOD/ZnO IOPCs modified FTO electrode (ZnO IOPCs modified electrode) and the Nafion/GOD/ZnO thin film modified FTO electrode (ZnO thin film modified electrode). Both the calibration curves of the ZnO IOPCs modified electrode and the ZnO thin film modified electrode show a linear response ranging from 0 mM to 10 mM. With the successive injection of glucose solution, the current of the ZnO IOPCs modified electrode obviously increased faster than the reference thin film electrode. The sensitivity of the ZnO IOPCs modified electrode was 8.62 μA mM^{-1} cm^{-2}, which was 18 times than 0.46 μA mM^{-1} cm^{-2} using the ZnO thin film modified electrode.

The increase of sensitivity of the ZnO IOPCs modified electrode can be attributed to two reasons: a large surface area of IOPC structure and the short diffuse distance for electron. Due to the macroporous structure of ZnO IOPCs, the surface area was quite large. At the same time, because the diameter of the pore was far bigger than the size of GOD, the GOD proteins could easily traverse through the pore canal and were adsorbed on the inwall of ZnO IOPCs. On the contrary, the ZnO thin film modified electrode can only adsorb GODs on the surface of the thin film. The amount of GOD adsorbed on the ZnO IOPCs modified electrode was much more than the reference thin film electrode. For ZnO IOPCs modified electrode, more GODs were adsorbed on the inwall of pore structure than the surface, and the diffuse distance from the inwall of pore structure was shorter than the surface, which reduced the recombination of electrons and defects or holes in the transition process and increased the value of forward current.

Then two experiments were designed for investigating what factors could influence the sensitivity of electrodes. In the first one, three electrodes with different thicknesses were made, named as ZnO IOPCs S1, ZnO IOPCs S2 and ZnO IOPCs S3 using the same pore size PMMA templates, and their thicknesses were 1.8, 2.8 and 4.2 μm, respectively. Fig. 4a indicated that the sensitivity increased as the thickness changed from 1.8 to 4.2 μm, and the linearity of ZnO IOPCs S3 was better than the others. With the thickness increasing, the electrodes adsorbed larger amount of GOD on the inwall of the pore structure and surface, so the current of ZnO IOPCs S3 was bigger and more stable than the two others. In the second, four electrodes with PSB positions of 520, 548, 606, and 640 nm were prepared, and named as IOPCs 520, IOPCs 548, IOPCs 606 and

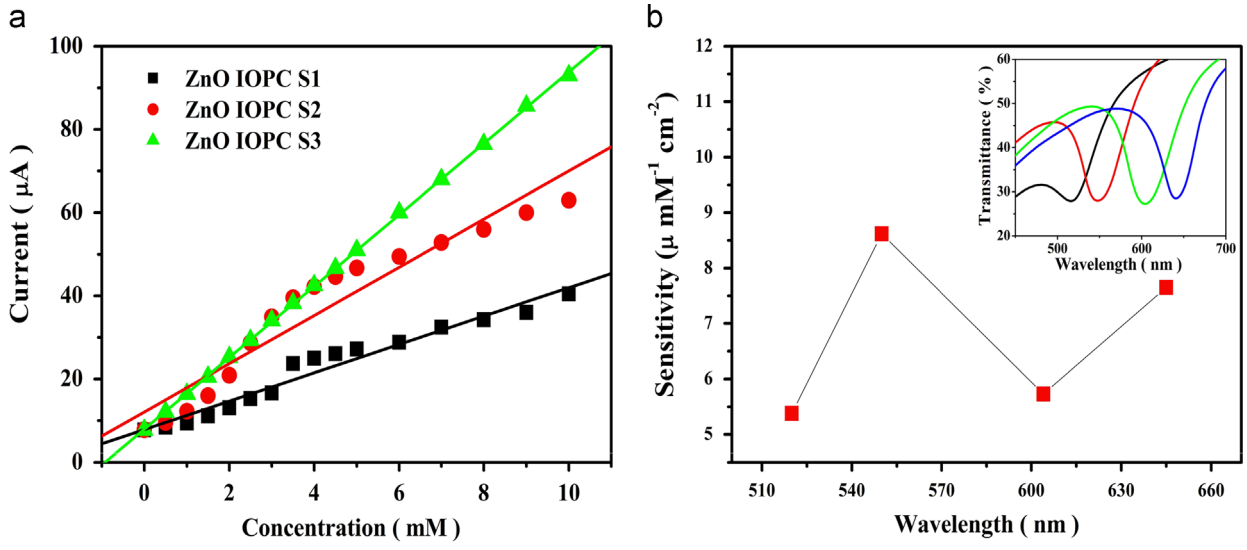

Fig. 4. (a) Calibration curves of amperometric response of ZnO IOPCs S1, ZnO IOPCs S2 and ZnO IOPCs S3 to successive addition of glucose. (b) The sensitivity of ZnO IOPCs 520, ZnO IOPCs 548, ZnO IOPCs 606 and ZnO IOPCs 640 modified electrodes.

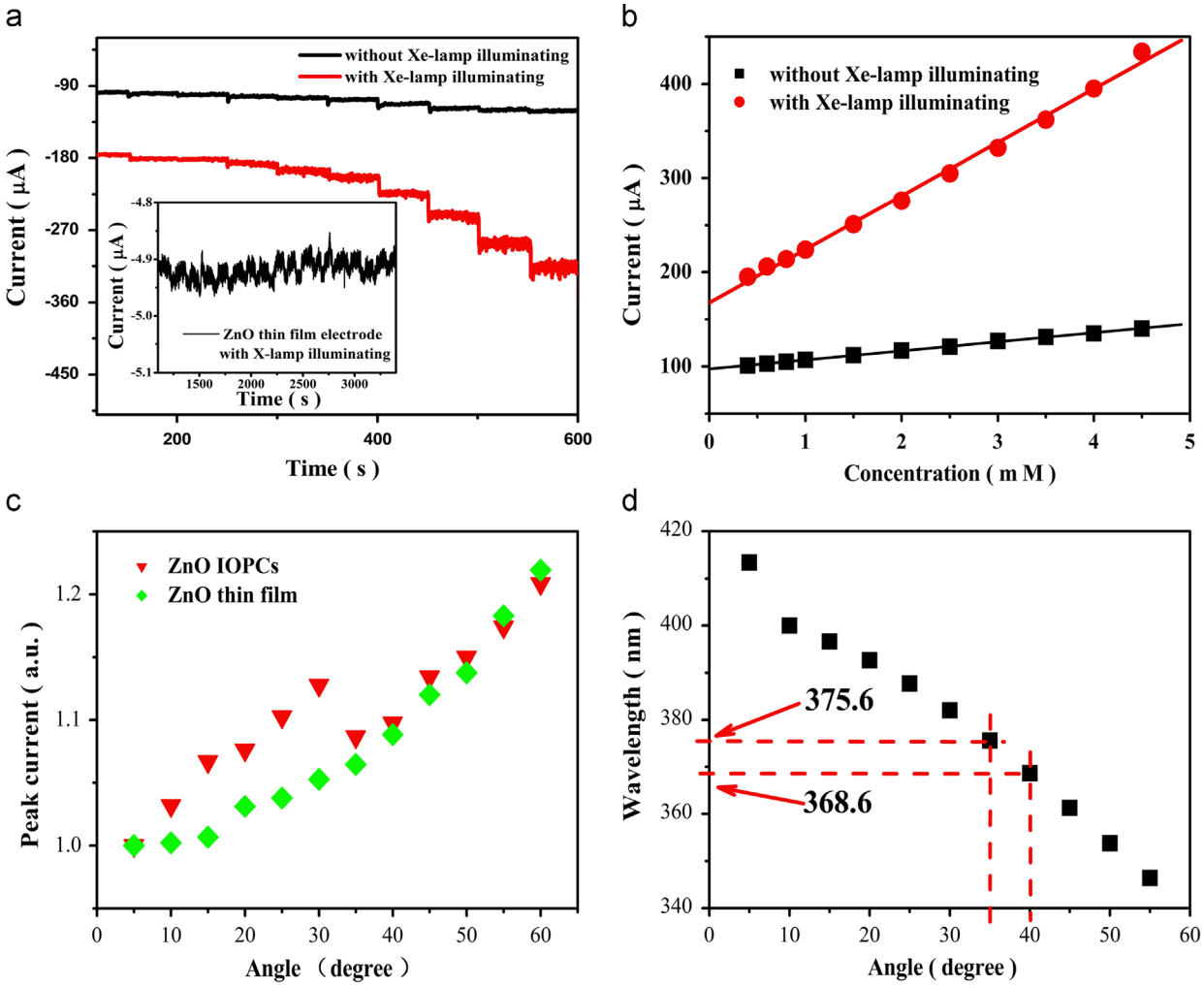

Fig. 5. (a) Amperometric response of ZnO IOPCs modified electrode with Xe-lamp illuminating and without Xe-lamp illuminating. (Inset) Amperometric response of ZnO thin film modified electrode with Xe-lamp illuminating (b) The corresponding calibration curves of (a). (c) The cathodic peak current of CV curves of ZnO IOPCs modified and ZnO thin film modified FTO electrodes with different incident angle. (d) The position of PSB with different incident angle of the ZnO IOPCs modified electrode.

IOPCs 640, respectively. The transmittance spectra of the four samples are shown in the inset picture of Fig. 4b, indicating that the four samples had good structure of IOPCs. As shown in Fig. 4b, the sensitivity of ZnO IOPCs 520, ZnO IOPCs 548, ZnO IOPCs 606 and ZnO IOPCs 640 was 5.38 $\mu A\ mM^{-1}\ cm^{-2}$, 8.62 $\mu A\ mM^{-1}\ cm^{-2}$, 5.73 $\mu A\ mM^{-1}\ cm^{-2}$ and 7.65 $\mu A\ mM^{-1}\ cm^{-2}$, respectively. There was no regular change with positions of PSB, illuminating that the pore size of IOPCs had no obvious influence on the sensitivity.

Because of the periodic structure of IOPCs, photoelectrochemical detection was developed for further improving the sensitivity. Fig. 5a displays *I–t* curves of the photoelectrochemical sensor for successive addition of glucose with Xe-lamp illumination and without Xe-lamp illumination. It indicated that the Nafion/GOD/ZnO IOPCs modified FTO electrodes had a fast electrochemical response to the glucose. Fig. 5b shows their corresponding calibration curves. Two linear relationships between response and glucose concentration were deduced. From the slope of the lines, the sensitivity with Xe-lamp illumination was 52.4 $\mu A\ mM^{-1}\ cm^{-2}$, which was about four times to the one without Xe-lamp illumination (14.1 $\mu A\ mM^{-1}\ cm^{-2}$), indicating that the ZnO IOPCs modified electrodes obviously improved the sensitivity with Xe-lamp illumination in glucose detection. However, when using ZnO thin film modified electrodes, the current almost remained unchanged with Xe-lamp illumination. As shown in the inset picture of Fig. 5a, the current increased immediately after glucose added, and it gradually tended to stable state after about 100 s.

Since the ZnO electronic band gap is around 3.2 eV, corresponding to a wavelength of around 380 nm, when the wavelength of the illumination light is less than 380 nm, electrons can transit from the valance band to the conduction band, so there are lots of electrons on the surface of the ZnO nanoparticles. For the thin film electrode, the nanoparticles are close packed inside the thin film. When the electrode was illuminated, there were a large amount of electrons generating inside the thin film, and the electron concentration tended to saturate, which inhibited the electrons generated in the oxidation–reduction reactions transferring from the surface of the thin film to the inside and meanwhile due to electron concentration gradient between the inside and the surface of the thin film, the electrons inside transferred to the surface and generated the reverse current. After a while, the electron concentration gradient gradually disappeared, and the electron concentration of the inside and the surface kept balance, so the current reached a steady value. For the IOPCs electrode, the GOD was adsorbed on the surface and inwall of the porous structure of the IOPCs, when the electrode was illuminated by Xe-lamp, the electrons generated on the surface and inwall of the IOPCs were immediately transferred to the FTO substrate under an extra electrical field. In other words, the photon-generated electrons increased the cathodic current and inhibited recombination of electrons and holes.

Because the structure of IOPCs could increase absorption of incident light of certain wavelength, we investigated how the change of PSB influenced on absorption of incident light. Previous

works confirm that the dependence of PSB in the transmittance spectra on incident angle fits well with Bragg's law, which can be expressed as (Zhu et al., 2012; Ren et al., 2006)

$$\lambda = 2\sqrt{\frac{2}{3}}D \times \sqrt{n^2_{eff} - \sin\theta^2}, \quad (3)$$

$$n_{eff} = n_{ZnO}\phi + n_{PBS}(1-\phi), \quad (4)$$

where λ is the wavelength derived from the PSB, D is the pore size of the IOPCs, θ is the angle of incidence light, n_{eff} is the effective refractive index of ZnO IOPCs, n_{ZnO} and n_{PBS} are the refractive index of ZnO and the PBS solution respectively, Φ is the ZnO IOPCs volume percentage, which is generally taken as 0.26. When $\lambda = 0^\circ$, the position of PSB of ZnO IOPCs is 414 nm. When λ change from 5° to 60°, the positions of PSB are calculated by Eqs. 1 and 2 as shown in Fig. 5d. Meanwhile, a ZnO thin film modified electrode was also made as a reference sample and tested in the same condition.

Fig. 5c shows the cathodic peak current (normalized at 5°) change with different incident light rotation angles when using the ZnO IOPCS and ZnO thin film modified electrodes. When using the thin film electrode, the cathodic peak current gradually increases with the incident light angle changing from 5° to 60°. This change may be caused by the increasing of effective optical transmission distance. When the light vertical incidents on the surface of the thin film electrode (incident angle=0°), the actual optical path is the most shortest; when the incident angle rotates from 5° to 60°, the actual optical path becomes longer.

For the ZnO IOPCS modified electrode, the cathodic reduction peak current similarly increases when the position of PSB shifts to the short wavelength side. However, the points of 375.6 nm and 368.6 nm are slightly smaller than the neighboring points, and the points which incident light angle changing from 10° to 30° are bigger than the reference thin film electrode. These phenomena could be attributed to slow light effect, which caused by the structure of IOPCs.

The slow light effect indicates that at photon energies approaching a PSB from the red side, the group velocity of light decreases and light can be increasingly described as a sinusoidal standing wave that has its highest amplitude in the high refractive index part of the structure (Nishimura et al., 2003; Chen et al., 2006). The fact that light waves are localized in different parts of the structure, depending on their energy, implies that an absorber in the high dielectric medium should interact more strongly with light at wavelength to the red of the stop band, and less strongly to the blue. So when the absorption peak of ZnO IOPCs locates at the red side of the PSB, light absorption of the ZnO IOPCS modified electrodes is stronger than that when the peak locates at the blue side of the PSB. But when the absorption peak overlaps the PSB, the group velocity of light is faster than that at the edge of the PSB, so we can see the points of 375.6 nm and 368.6 nm located within the PSB of ZnO IOPCs are smaller than the points at the edge of the PSB. And the absorption at the red side of the PSB of ZnO IOPCs (10–30°) is stronger than the reference thin film electrode.

However, the enhancement of light absorption by slow light effect is only less than two times, so the multiple scattering in ZnO IOPCs may be the major reason for increasing the light absorption of ZnO IOPCS modified electrodes.

Table S1 shows a comparison of the detection range, sensitivity and stability of several typical enzymatic ZnO nanomaterials biosensor for glucose detection as well as the Nafion/GOD/ZnO IOPCs modified biosensor in our study. As compared, the Nafion/GOD/ZnO IOPCs modified biosensor exhibits satisfactory integrative performances.

2.5. Selectivity , reproducibility and stability

The Nafion/GOD/ZnO IOPCs modified FTO electrodes also exhibit excellent selectivity for glucose detection. As shown in Fig. S2, the addition of interferents, 0.1 mM of ascorbic acid (AA) and 0.1 mM of uric acid (UA), which are usually present in the biological fluid, gives rise to negligible current changes, while a significant current response is observed for the subsequent addition of 0.5 mM of glucose. The current ratios of AA to glucose were determined to be 2.5%, while current ratios of UA to glucose to be 1.67%. To assess its stability, Nafion/GOD/ZnO IOPCs modified FTO electrodes were stored at 4 °C in a dry state after use and used to measure the current response for 2 mM of glucose every day. The Nafion/GOD/ZnO IOPCs modified FTO electrode retains 91% of its original current response over a storage period of 2 weeks. For reproducibility, five Nafion/GOD/ZnO IOPCs modified FTO electrodes were separately prepared under the same conditions, the relative standard deviations (RSDs) were calculated to be no more than 6.5% (data is not shown).

3. Conclusions

We synthesized ZnO IOPCs by the sol–gel method using the PMMA as a template, then Nafion/GOD/ZnO IOPCs modified FTO electrodes were fabricated and their biosensing properties were carefully studied. The results demonstrated that the sensitivity of ZnO IOPCs modified electrode was 18 times than that using ZnO thin film modified electrode, due to the porous structure of IOPCs with a large surface area. For photoelectrochemical detection, the sensitivity was reached up to 52.4 $\mu A\,mM^{-1}\,cm^{-2}$, which was almost four times to the one without illumination (14.1 $\mu A\,mM^{-1}\,cm^{-2}$). The reason can be attributed to the slow light effect and multiple scattering of IOPCs structure. Moreover, it also showed strong stability, good reproducibility and an excellent selectivity. Overall, the Nafion/GOD/ZnO IOPCs modified FTO electrodes exhibit great potential for the application of enzymatic photoelectrochemical glucose biosensor.

Acknowledgments

This work was supported by National Talent Youth Science Foundation of China (Grant no. 60925018), the National Natural Science Foundation of China (Grant nos. 61204015, 51002062, 11174111, 61177042, and 81201738), the Open Research Fund of State Key Laboratory of Bioelectronics, Southeast University, the Opened Fund of the State Key Laboratory on Integrated Optoelectronics (No. IOSKL2012KF04), the Jilin Province Natural Science Foundation of China (No. 20140101171JC) and the China Postdoctoral Science Foundation Funded Project (2012M511337 and 2013T60327).

Appendix A. Supporting information

Supplementary data associated with this article can be found in the online version at http://dx.doi.org/10.1016/j.bios.2014.03.038.

References

Asif, M.H., Ali, S.M., Nur, O., Willander, M., Brnnmark, C., Strlfors, P., Englund, U.H., 2010. Biosens. Bioelectron. 25 (10), 2205–2211.
Arpin, K.A., Mihi, A., Johnson, H.T., Baca, A.J., Rogers, J.A., Lewis, J.A., Braun, P.V., 2010. Adv. Mater. 22 (10), 1084–1101.
Baba, T., 2008. Nature Photonics 2, 465–473.
Bao, S.J., Li, C.M., Zang, J.F., Cui, X.Q., Qiao, Y., Guo, J., 2008. Adv. Funct. Mater. 18 (4), 591–599.

Chen, H., Chen, S., Quan, X., Zhang, Y.B., 2010a. Environ. Sci. Technol. 44 (1), 451–455.
Chen, J.I.L., Freymann, G., von, Choi, S.Y., Kitaev, V., Ozin, G.A., 2006. Adv. Mater. 18 (14), 1915–1919.
Chen, J.I.L., Freymann, G., von, Kitaev, V., Ozin, G.A., 2007. J. Am. Chem. Soc. 129 (5), 1196–1202.
Chen, J.I.L., Loso, E., Ebrahim, N., Ozin, G.A., 2008. J. Am. Chem. Soc. 130 (16), 5420–5421.
Chen, X.Q., Li, Z.S., Ye, J.H., Zou, Z.G., 2010b. Chem. Mater. 22 (12), 3583–3585.
Dai, Z.H., Shao, G.J., Hong, J.M., Bao, J.C., Shen, J., 2009. Biosens. Bioelectron. 24 (5), 1286–1291.
Fang, B., Gu, A.X., Wang, G.F., Wang, W., Feng, Y.H., Zhang, C.H., Zhang, X.J., 2009. ACS Appl. Mater. Interfaces 1 (12), 2829–2834.
Fang, B., Zhang, C.H., Wang, G.F., Wang, M.F., Ji, Y.L., 2011. Sens. Actuators B 155 (1), 304–310.
Hu, W.H., Liu, Y.S., Zhu, Z.H., Yang, H.B., Li, C.M., 2010. ACS Appl. Mater. Interfaces 2 (6), 1569–1572.
Joannopoulos, J.D., Johnson, S.G., Winn, J.N., Meade, R.D., 2008. Photonic Crystals: Molding the Flow of Light. Princeton University Press, Princeton.
Lee, D., Lee, J., Kim, J., Na, H.B., Kim, B., Shin, C.H., Kwak, J.H., Dohnalkova, A., Grate, J.W., Hyeon, T., Kim, H.S., 2005. Adv. Mater. 17 (23), 2828–2833.
Lee, S.-H.A., Abrams, N.M., Hoertz, P.G., Barber, G.D., Halaoui, L.I., Mallouk, T.E., 2008. J. Phys. Chem. B 112 (46), 14415–14421.
Li, C.M., Dong, H., Cao, X., Luong, J.H., Zhang, X., 2007. Curr. Med.Chem. 14 (8), 937–951.
Liao, G.Z., Chen, S., Quan, X., Chen, H., Zhang, Y.B., 2010. Environ. Sci. Technol. 44 (9), 3481–3485.
Liu, Y., Wang, M., Zhao, F., Xu, Z.A., Dong, S.J., 2005. Biosens. Bioelectron. 21 (6), 984–988.
Mu, C., Zhao, Q., Xu, D., Zhuang, Q., Shao, Y., 2007. J. Phys. Chem. B 111 (6), 1491–1495.
Nishimura, S., Abrams, N., Lewis, B.A., Halaoui, L.I., Mallouk, T.E., Benkstein, K.D., Lagemaat, J.V.D., Frank, A.J., 2003. J. Am. Chem. Soc. 125 (20), 6306–6310.
Rakow, N.A., Suslick, K.S., 2000. Nature 406, 710–713.
Ren, M.M., Ravikrishna, R., Valsaraj, K.T., 2006. Environ. Sci. Technol. 40 (22), 7029–7033.
Riklin, A., Katz, E., Willner, I., Stocker, A., Buchmann, A.F., 1995. Nature 376, 672–675.
Sakoda, K., 1999. Opt. Express 4 (5), 167–176.
Shan, D., Zhu, M.J., Xue, H.G., Cosnier, S., 2007. Biosens. Bioelectron. 22 (8), 1612–1617.
Umar, A., Rahman, M.M., Kim, S.H., Hahn, Y.B., 2008. J. Nanosci. Nanotechnol. 8 (6), 3216–3221.
Vinu, A., Miyahara, M., Ariga, K., 2005. J. Phys. Chem. B 109 (13), 6436–6441.
Wang, Joseph, 2008. Chem. Rev. 108, 814–825.
Wang, J.X., Sun, X.W., Wei, A., Lei, Y., Cai, X.P., Li, C.M., Dong, Z.L., 2006. Appl. Phys. Lett. 88 (23), 233106–233108.
Wei, A., Sun, X.W., Wang, J.X., Lei, Y., Cai, X.P., Li, C.M., Dong, Z.L., Huang, W., 2006. Appl. Phys. Lett. 89 (12), 123902–123904.
Wen, X.G., Xie, Y.T., Mak, M.W.C., Cheung, K.Y., Li, X.Y., Renneberg, R., Yang, S.H., 2006. Langmuir 22 (10), 4836–4842.
Wu, S., Ju, H.X., Liu, Y., 2007. Adv. Funct. Mater. 17, 585–592.
Xian, Y.Z., Yi, H., Liu, F., Xian, Y., Wang, H.T., Jin, L.T., 2006. Biosens. Bioelectron. 21 (10), 1996–2000.
Yang, P., Zhao, D., Margolese, D.I., Chmelka, B.F., Stucky, G.D., 1998. Nature 396, 152–155.
Zang, J.F., Li, C.M., Cui, X.Q., Wang, J.X., Sun, X.W., Dong, H., Sun, C.Q., 2007. Electroanalysis 19 (9), 1008–1014.
Zhang, F.F., Wang, X.L., Ai, S.Y., Sun, Z.D., Wan, Q., Zhu, Z.Q., Xian, Y.Z., Jin, L.T., Yamamoto, K., 2004. Anal. Chim. Acta 519 (2), 155–160.
Zhang, S.X., Wang, N., Niu, Y.M., Sun, C.Q., 2005. Sens. Actuators B 109 (2), 367–374.
Zhao, S., Zhang, K., Bai, Y., Yang, W.W., Sun, C., 2006. Bioelectrochemistry 69 (2), 158–163.
Zhao, Z.W., Chen, X.J., Tay, B.K., Chen, J.S., Han, Z.J., Khor, K.A., 2007. Biosens. Bioelectron. 23 (1), 135–139.
Zhu, H.G., Stein, E.W., Lu, Z.H., Lvov, Y.M., McShane, M.J., 2005. Chem. Mater. 17 (9), 2323–2328.
Zhu, X.L., Yuri, I., Gan, X., Suzuki, I., Li, G.X., 2007. Biosens. Bioelectron. 22 (8), 1600–1604.
Zhu, Y.S., Xu, W., Zhang, H.Z., Wang, W., Xu, S., Song, H.W., 2012. J. Phys. Chem. C 116 (3), 2297–2302.